Scientific Reports

https://doi.org/10.1038/s41598-026-43121-7

Article in Press

Lake bathymetric reconstruction and water storage estimation method based on terrain feature similarity

Received: 16 October 2025

Accepted: 2 March 2026

Published online: 26 March 2026

Cite this article as: Zhang X., Qi C., Xu D. *et al.* Lake bathymetric reconstruction and water storage estimation method based on terrain feature similarity. *Sci Rep* (2026). https://doi.org/10.1038/s41598-026-43121-7

Xuteng Zhang, Changxian Qi, Dezhong Xu, Yao Chen, Hongjun Li & Haiyue Peng

Lake Bathymetric Reconstruction and Water Storage Estimation Method Based on Terrain Feature Similarity

Xuteng Zhang[2, 3, 4], Changxian Qi[1], Dezhong Xu[1],Yao Chen[1], Hongjun Li[1], Haiyue Peng[1, 2, 3, 4, *]

1. China Geological Survey, Xining Natural Resources Comprehensive Survey Center, Xining 810021, China;
2. School of Civil Engineering and Water Resources, Qinghai University, Xining 810016, China;
3. Laboratory of Water Ecological Management and Protection in River Source Areas, Ministry of Water Resources, Xining 810016, China;
4. State Key Laboratory of Plateau Ecology and Agriculture, Xining 810016, China.

* Correspondence: YS220815020227@qhu.edu.cn

Abstract

Closed-basin lake hydrological elements serve as important indicators of climate change. However, because of natural constraints and limited monitoring conditions, the hydrological information (such as area, water level, and storage) of lakes on the Qinghai–Tibet Plateau remains insufficiently understood, which poses challenges in the quantitative assessment of lake water storage and its variations. In this study, a lake water storage estimation method that is based on surrounding topographic parameters is proposed. By calculating and extrapolating terrain parameters such as slope variations around the lake, a reasonably accurate digital representation of underwater topography can be obtained, enabling the quantitative evaluation of lake water storage. Nine lakes on the Qinghai–Tibet Plateau with available monitoring or research data are selected to verify the applicability and accuracy of the proposed method. The results reveal that the relative errors of the simulated maximum water depth range from 8% to 47%, with larger errors observed for Yamdrok Lake and Dongge Co'nag. The relative errors of the simulated average water depth range from 7.5% to 47%, with greater deviations observed for Xingxinghai and Kuhai Lake. For Ra'ang Co, Cuoe Lake, Anglaren Co, and Mapam Yumco, the relative error of comparison with the measured points is less than 20%. The model incorporates multiple functional forms and multidirectional profile combinations, rendering the results more consistent with actual geomorphological characteristics and robust to topographic noise. This study provides a useful reference for estimating water storage in lakes lacking measured data on the underwater topography.

Keywords: Lake Water Storage Estimation; Digital Elevation Model (DEM); Digital Underwater Terrain; Tibetan Plateau

1. Introduction

Lakes play important roles in shaping the hydrological cycle (Pi et al., 2022) and directly participate in regional and global water circulation processes (Verpoorter et al., 2014; Woolway et al., 2020). These bodies of water serve as key factors in assessing regional water resource availability and maintaining regional ecosystems (Qin et al., 2020; Song et al., 2013; Yao et al., 2018). In recent years, with the continuous rise in global temperatures, climate change on the Qinghai–Tibet Plateau has become particularly pronounced (Dai et al., 2024; Zhang et al., 2024; Zhang et al., 2014). Precipitation has increased annually, and the melting rate of glaciers and permafrost has accelerated (Zhang et al., 2015), leading to dramatic changes in lakes across the plateau. These changes inevitably affect local residents and surrounding engineering facilities (Dawa et al., 2010), and the increase in stored lake water simultaneously increases the risk of dam failure. Lake bathymetry is an indispensable parameter for lake water volume estimation, but underwater terrain measurement is expensive. On the Qinghai–Tibet Plateau, owing to terrain and transportation constraints, more than 95% of lakes lack bathymetric data,

resulting in unclear water storage estimates. Since the 19th century, scientists have begun studying water volume variations in lakes on the plateau. The Swedish geographer Sven Hedin repeatedly visited the plateau and conducted basic surveys of individual lakes. After the founding of the People's Republic of China, two large-scale scientific expeditions to the plateau were conducted, and their results provided valuable data for subsequent research. The harsh geological conditions and high altitude of the Qinghai–Tibet Plateau have left only a few lakes with measurable bathymetric data (Moses et al., 2013; Zhu et al., 2017). The number of lakes observed via the use of traditional hydrological monitoring methods is highly limited compared with the vast number of lakes on the plateau (Zhang et al., 2014).

To estimate the water storage capacities of lakes without measurable data, various methods have been proposed. A combination of hydrological models and measured data can effectively simulate changes in lake water volume. Zhou et al., considering water balance, applied the Water and Energy Budget-based Distributed Hydrological Model (WEB–DHM) combined with two different evapotranspiration algorithms to study water volume variations in Siling Co between 2003 and 2012 (Zhou et al., 2015). However, in remote areas such as the Qinghai–Tibet Plateau, measuring data is extremely difficult. The development of satellite remote sensing technology has provided a solution to this issue (Zhang et al., 2020; Calkoen et al., 2001; Bian et al., 2017). Xu et al. used GRACE satellite-derived terrestrial water storage data and residuals simulated by two hydrological models, namely, Global Land Data Assimilation System (GLDAS) Noah and WaterGAP Global Hydrology Model (WGHM), to estimate the water volume variations in Poyang Lake (Xu et al., 2020). Combined altimetry satellites and optical imagery can be used to determine the lake area–water level relationship. Wang Wenzhong et al. employed Sentinel-3A data from 2016–2018 as the sole water level data source, combined with Landsat optical imagery, to estimate water volume changes in Tangra Yumco and subsequently explored possible drivers of lake changes via the use of GLDAS product data (Wang et al., 2020). Alternatively, spectral characteristics can be used to invert shallow water depths. Bo et al. applied convolutional neural networks (CNNs) to retrieve water depths from remote sensing imagery, achieving high accuracy within 5 m (Ai et al., 2020). However, spectral methods are limited by water transparency and maximum penetration depth, making them ineffective in turbid or deep-water regions (Lyzenga et al., 1981; Collin et al., 2012; Moses et al., 2013). Synthetic aperture radar (SAR) is affected by conditions such as wind and waves, and the data coverage is limited (Alpers et al., 1984; Shuchman et al., 1985; Kg et al., 2008). Statistical and empirical formula methods can be used to establish relationships between lake basin parameters, such as maximum depth and average depth, and measurable physical quantities, such as slope and aspect, thereby allowing the estimation of lake water volume (Hollister et al., 2011; Messager et al., 2016). These methods are cost effective but often limited by the generalizability of the empirical formulas. O'Connor and Huggel et al. proposed different empirical models that provide the lake water volume through empirical relationships between the lake depth and surface area (O'Connor et al., 2001; Yang et al., 2024).

In recent years, methods based on the geological continuity hypothesis and the use of digital elevation models (DEMs) of the surroundings to extrapolate underwater topography have shown great potential (Fang et al., 2023; Zhu et al., 2019). However, most existing DEM interpolation or empirical methods have significant limitations: in previous studies, scholars typically performed topography extrapolation or profile calculations on a single profile without fully considering the combined impact of the surrounding topography in multiple directions, leading to inaccurate topographic characterization of lakes with complex geological conditions and thereby affecting reconstruction accuracy. To overcome these limitations, an innovative underwater topography construction method is proposed in this study, with the core innovation being the integration of a multidirectional profile combination iterative algorithm with a function library. This model abandons the traditional single-direction recursive calculation and instead relies on a four-neighbourhood-based multidirectional profile synchronous calculation and iterative advancement mechanism that enhances the adaptability of the model to complex terrain and makes the reconstruction results more consistent with the actual spatial topography. Moreover, by considering the complex and variable nature of lake basins, the model incorporates a function library

with various forms, including quadratic functions, exponential functions, and trigonometric functions, which can adaptively select the optimal fitting function for different topographic profiles during the iteration process, thus accurately simulating the underlying topography. The combination of these two approaches effectively increases the simulation accuracy of the model. In this study, nine representative lakes on the Qinghai–Tibet Plateau are selected for validation to assess the applicability and accuracy of the method in complex geographic environments and under diverse lake basin conditions.

2. Study Area and Data Sources

2.1 Study Area Overview

The Qinghai–Tibet Plateau contains many lakes, with more than 1,400 lakes exceeding 1 km² in area. The total lake area is approximately 5×10^4 km², accounting for approximately 50% of the total lake area in China (Yao et al., 2022). However, owing to inconvenient transportation and the limited accessibility of large-scale survey equipment, more than 95% of the lakes on the plateau lack bathymetric data. In this study, nine representative lakes on the Qinghai–Tibet Plateau were selected for validation (Figure 1) to assess the applicability of the proposed method across diverse environmental settings.The selected lakes vary in size and are distributed across different geographic units of the plateau. Additionally, the shoreline shapes and surrounding topographic features of these lakes significantly differ, including those of lakes with highly complex shorelines and steep slope zones, providing an ideal testing scenario for evaluating the adaptability of the model under complex terrain conditions. The availability of data are considered. Specifically, some lakes have measurable depth data, which can be used for pixel-by-pixel validation. However, in other lakes, water storage data are estimated by different methods; these data can be cross-validated and compared with the model simulation results.

2.2 Data Sources

DEM data, as important carriers of topographic information, can accurately provide key terrain parameters such as slope, aspect, boundary contour, and water surface elevation around lakes. These parameters play significant roles in the model. Water surface elevation and the lake boundary jointly determine the initial conditions and spatial range for model calculations. Slope and aspect are core input parameters that directly participate in the profile fitting of the underwater terrain. In this study, the Shuttle Radar Topography Mission (SRTM) DEM V3 data version provided by the U.S. Geological Survey is used, with a spatial resolution of 90 m (data source: https://earthexplorer.usgs.gov/). This dataset has a high precision, low root mean square error, and minimal data gaps. The SRTM DEM has been repeatedly validated in Asia, demonstrating good data reliability.

The basic geographic information of the lakes is sourced from the National Tibetan Plateau Data Centre (https://data.tpdc.ac.cn/home). In this study, a dataset of lakes larger than 0.01 km² on the Qinghai–Tibet Plateau (2016–2021) (Yang et al., 2022) is used to systematically catalogue the spatial distribution information of lakes on the plateau. Lake water level data are selected from the dataset of water level changes in major lakes of the Qinghai–Tibet Plateau (Peng et al., 2022), which are used to calculate lake water storage.

To systematically evaluate the reconstruction accuracy of this model, water depth data for four lakes, namely, Ra’ang Co, Cuoe Lake, Anglaren Co, and Mapam Yumco, are collected (Wang, 2018). Data are measured using the Lowrance HDS-5 sonar depth sounder, providing one or more representative sets of lakebed profile data, which can be used for pixel-by-pixel error analysis of the underwater terrain output of the model, objectively reflecting the performance of the model for lakes with different basin shapes. Moreover, to assess the performance of the model in terms of water storage estimation, a simulated lake water storage dataset constructed by Han et al. (2024), which is based on ICESat-2 laser altimetry data and a self-affine theoretical empirical equation, is selected for cross-validation with the model results.

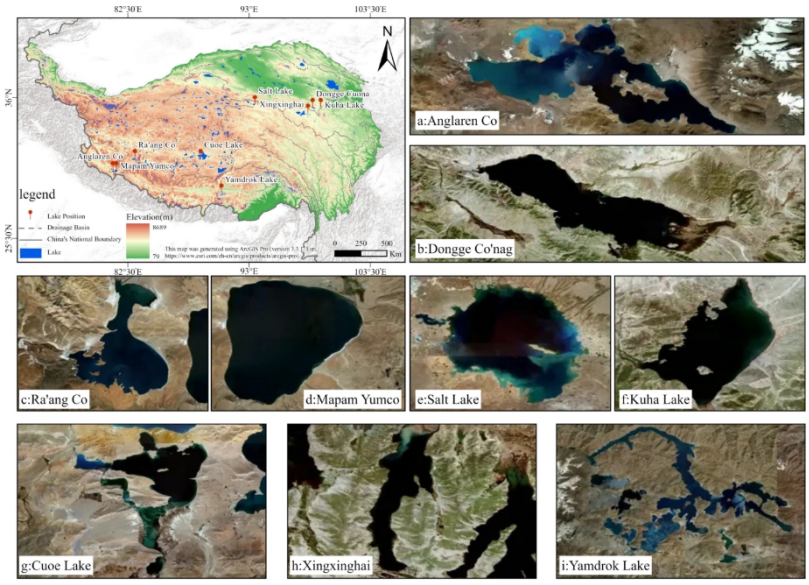

Figure 1. Geographic locations and lake morphologies of the validated lakes.

3. Research Methods

3.1 Construction of Lake Underwater Digital Topography

3.1.1 Methodological Principle

On the basis of the geological continuity hypothesis, lake bathymetry is regarded as a natural extension of terrestrial terrain, and the underlying topography can be inferred from the surrounding landforms. However, most extrapolated areas of lakes lack sufficient known depth points to serve as strong constraints, which introduces considerable uncertainty into the extrapolation process. To avoid generating unrealistic bathymetric features, it is necessary to rely on reasonable assumptions and mathematical models to ensure that the extrapolated results are consistent with the actual terrain. For example, the slope characteristics of lakes often exhibit high spatial variability, and the attenuation rates of slope gradients differ across regions. In addition, multiple geomorphic types can exist beneath the lake surface. Steep-slope regions typically exhibit rapid slope changes and depth attenuation rates, as shown in Figures 2(A) and (C), whereas shoal areas generally have gentler gradients, with relatively slow changes in water depth, as shown in Figure 2(B). To accurately simulate bathymetry, the model must incorporate slope attenuation mechanisms adapted to different geomorphic features, thereby accommodating spatial heterogeneity in terrain characteristics.

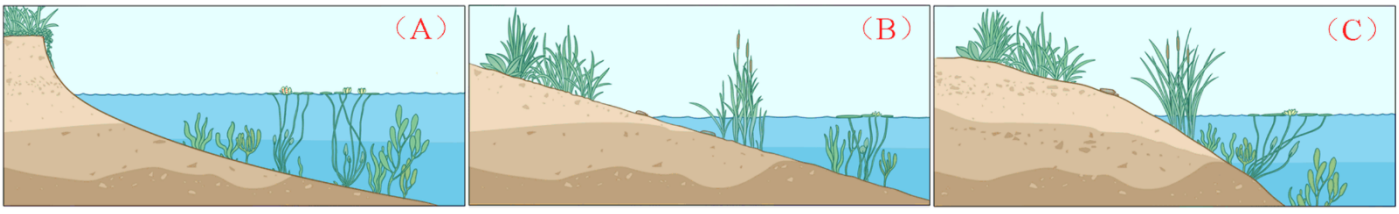

Figure 2. Slope characteristics of three typical lake slopes.

Referring to the assumption proposed by Zhu et al., the terrain of the land surface surrounding a lake can be used as a predictive factor for lake depth (Zhu et al., 2019). The results simulated via the use of this method represent the natural underwater surface of the lake. Existing bathymetric measurement techniques generally measure only the surface of the sediment layer, while sedimentation and erosion occur continuously and play significant roles in driving the long-term evolution of geomorphology. Sedimentation rates are often influenced by upstream geological conditions, climate, and vegetation,

making accurate prediction difficult. Therefore, the concept of a sedimentation coefficient is introduced to predict the thickness of the sediment layer.

3.1.2 Construction of Underwater Digital Topography

The model computation workflow is shown in Figure 3. DEM data are used as inputs, and after four key steps, i.e., data preprocessing, identification of potential calculation points, elevation calculation, and sedimentation calculation, the output is the underwater digital topography of the lake. The relevant parameters and their definitions are presented in Table 1.

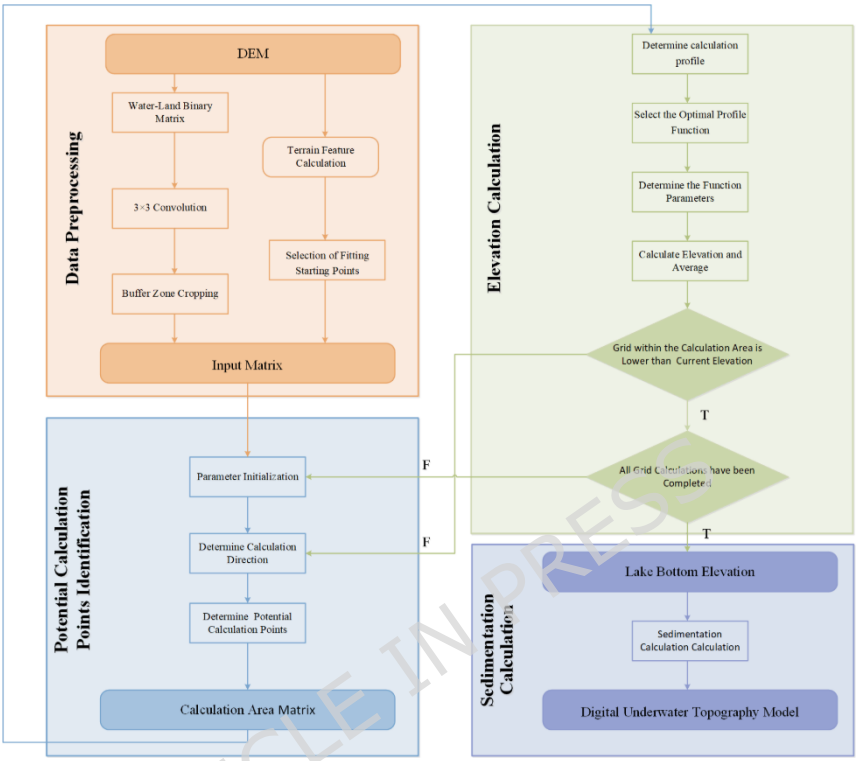

Figure 3. Model calculation flow chart.

Table. Table 1. Model parameters.

Variable Name	Parameter Name	Description
WL_MX	Water–Land Binary Matrix	Binarized matrix used to distinguish water bodies from land.
Buf	Buffer Zone	Terrestrial area correlated with lake depth.
GTF	Geomorphological Feature	Slope variations of terrain in different directions.
Fitting_Point	Fitting Starting Point	Pixel that determines the number of input datapoints for the fitting function.
Input_MX	Input Matrix	Dataset of slope variations cropped by the buffer zone.
Calc_EL	Current Calculation Elevation	Elevation corresponding to the current computation in the outer loop.
Step_L	Descent Step Length	Height decrease at the current elevation after each outer loop iteration.
Calc_Area	Computed Area	Binary matrix recording regions where elevations have already been computed.
Pot_Calc_Point	Potential Calculation Point	Points to be calculated within uncomputed regions that are determined using the four-neighbour method.

Variable Name	Parameter Name	Description
Calc_Dir	Calculation Direction	Direction adjacent to the computed area centred on the current calculation point.
Calc_Sec	Current Calculation Profile	Profile determined by the current calculation point and its direction.
Func_Form	Optimal Function Form	Function type selected from the function library that yields the best fitting result.
Func_Param	Optimal Function Parameters	Parameters of the optimal function determined through least squares fitting.
DUTM	Digital Underwater Topography Model	Predicted output of the model, where each pixel records an elevation value.

Computation Process:

(1) Data Preprocessing

As shown in Figure 4, data preprocessing includes water–land binary matrix division, 3×3 convolution, buffer zone cropping, terrain feature calculation, and selection of fitting starting points.

In the DEM, water pixels are assigned lake surface elevation values (Merryman et al., 2016). Via the use of the surface elevation as a threshold condition, a water–land binary matrix is generated. A 3×3 convolution is then applied to the binary matrix to emphasize the main water body and prevent fragmented pixels from interfering with subsequent calculations. Previous studies have revealed that the maximum depth of different lakes and related parameters are closely associated with slope variations at varying distances from the lake shore and that this distance is correlated with the lake surface area (Heathcote et al., 2015). To address this issue, a proportional buffer zone scaling method based on lake size is applied for data cropping. This method reduces the amount of data input into the model and prevents the inclusion of irrelevant terrain data in small lakes or the omission of critical topographic information in large lakes. The buffer zone calculation formula is as follows:

$$D = 2 \bullet \sqrt{\frac{A}{\pi}} \quad (1)$$

where D represents the equivalent diameter, m, and A denotes the lake area, m^2. The optimal buffer zone sizes are 25%, 50%, 75%, and 100% of the equivalent diameter.

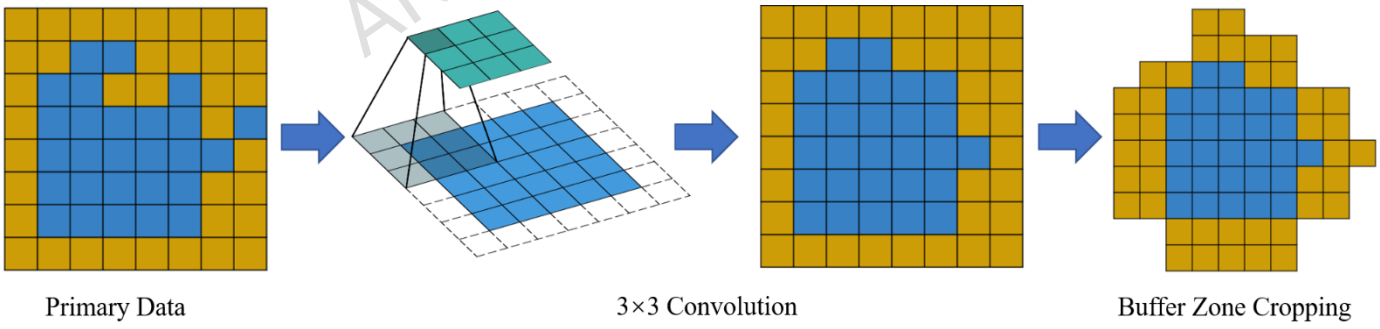

Figure 4. Buffer clipping diagram.

When the lake bathymetry is extrapolated from the surrounding terrain, the use of slope can avoid unreasonable outcomes that may result from direct elevation extrapolation, and the slope should be averaged along the direction perpendicular to the computation direction. The cross-shaped (four-neighbourhood) slope calculation method is as follows:

$$P(i) = \frac{H4\text{-}H10}{cellsize} \quad (2)$$

$$k_i = \sum_{i=1}^{n} P(i)/n \quad (3)$$

where *H4* and *H10* correspond to pixel elevations, m; cellsize denotes the raster resolution, m; and k_i represents the average slope of the pixel. During the computation process, regions containing water pixels are excluded from the slope calculation, as shown by pixel *H3* in Figure 5.

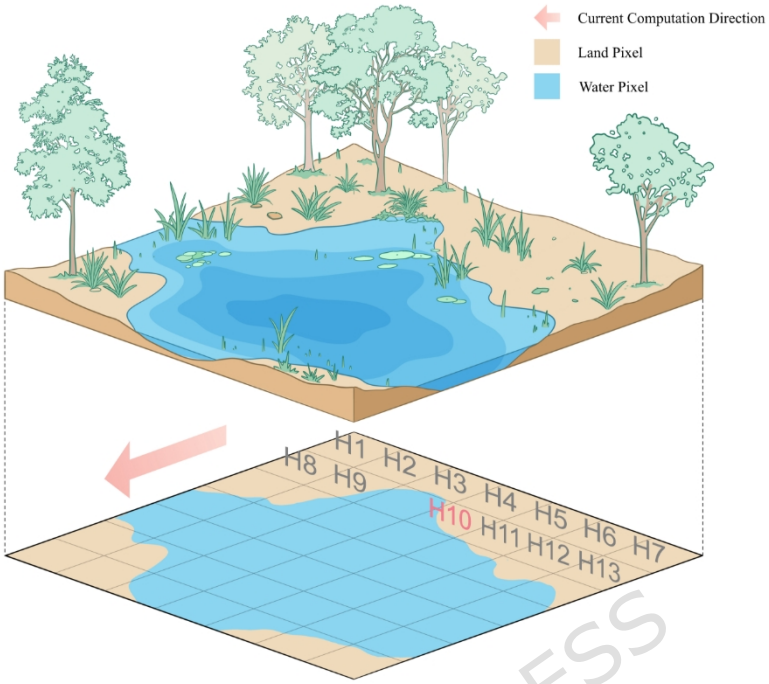

Figure 5. Slope calculation diagram.

Lake bathymetry construction can be regarded as a complex combination of profiles in multiple directions. Each single direction (profile) can be simplified as a two-dimensional extrapolation problem. Constrained by geological theory, selecting either too many or too few fitting pixels may lead to inaccurate fitting outcomes. Therefore, the number of data points involved in the fitting is critically important. As shown in Figure 6, the criteria for selecting the fitting starting point include two conditions: (1) the slope of a land pixel changing from positive to negative or (2) the elevation difference of a pixel exceeding three times the mean elevation difference.

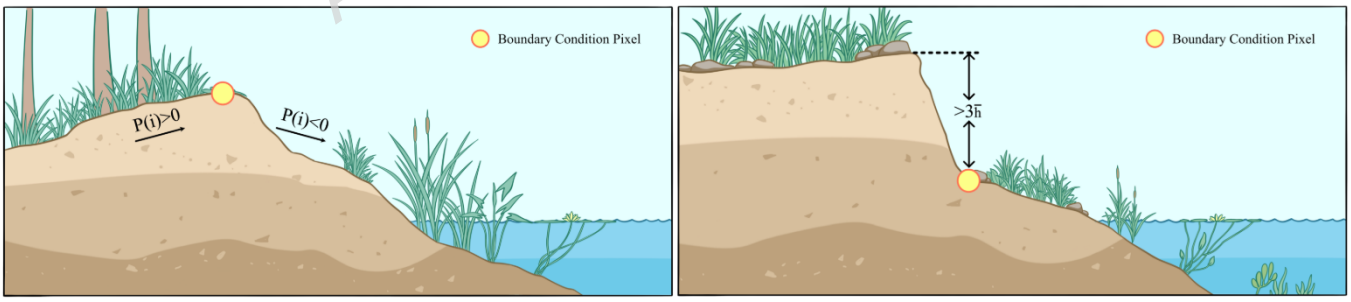

Figure 6. Fitting starting point selection diagram.

After appropriate fitting starting points are selected, they are superimposed onto the binary matrix to reduce the model data input and generate the final input matrix.

(2) Identification of Potential Calculation Points

Potential calculation points refer to all pixels that may participate in computation during the iterative loop of the model. Identifying these points is necessary to determine the current calculation matrix. The model employs a gradient descent approach to ensure that each computed result lies approximately on

the same elevation plane, thereby addressing potential discontinuities in elevation across the two-dimensional plane.

This model employs a nested two-layer iterative structure. It starts from the water surface elevation and gradually lowers the current elevation plane. Each time it lowers and completes all relevant calculations, it constitutes a complete elevation iteration round. Within each elevation plane, a set of multi-directional neighborhood-expansion iterative algorithms is used to calculate until the termination condition in that plane is met. This approach enhances the consistency of results with actual terrain relationships and maximizes the preservation of lake geomorphic features. In the elevation-iteration cycle (outer loop), the algorithm performs multi-directional expansion via elevation calculation (inner loop). The steps can be summarized as follows: (1) Starting from the determined starting point of calculation, determine the initial profile direction. (2) While advancing one pixel along this direction and performing elevation calculation, immediately expand one pixel in the orthogonal direction and identify it as a "potential calculation point". (3) If this "potential calculation point" meets the calculation conditions, it is immediately included in the calculation matrix of the current inner loop. (4) If the same pixel is repeatedly calculated, the arithmetic mean of its calculation results is taken as the final elevation of this pixel in the current elevation iteration round. (5) When the elevations of all pixels calculated in the inner loop are lower than the current elevation threshold set by the outer loop, the inner loop terminates for that round; subsequently, the outer loop decreases the elevation threshold by one step length and initiates a new round of the inner loop. Through this mechanism, the same pixel is calculated multiple times in different directions, and its final elevation integrates neighborhood information from these directions, thereby better reflecting the physical continuity of the actual terrain. As shown in Figure 7, the label 2-1 indicates the first elevation calculation within the second round of elevation iteration.

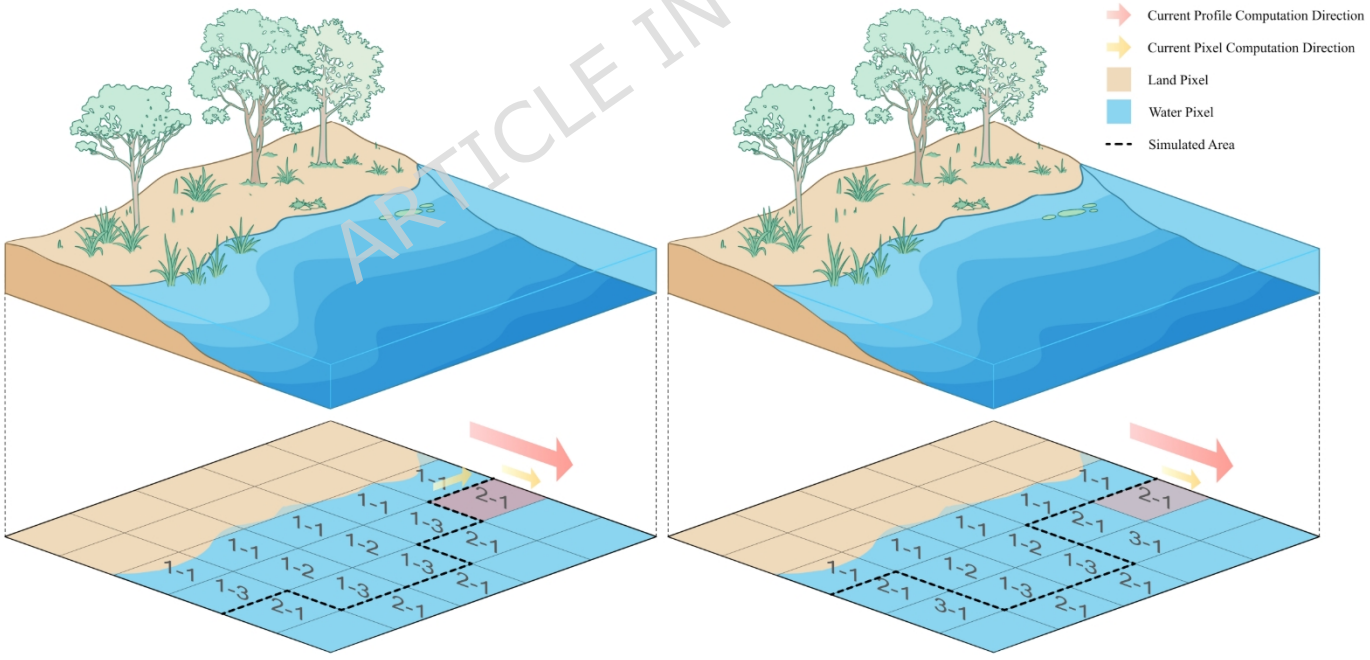

Figure 7. Model iteration diagram.

(3) Elevation Calculation

First, the current calculation profile is determined. Like in the inverse distance weighting method, only neighbouring units are used to estimate the elevation of the current calculation point. For example, as shown in Figure 5, the H10 pixel has adjacent directions to the right and upwards, while diagonal pixels are excluded.

After the calculation profile is determined, curve fitting is conducted using the least squares method. The experimental results indicate that when more than eight pixels are involved in the fitting process, terrain noise is easily introduced, whereas using fewer than two pixels leads to underfitting. Therefore, a flexible window range of 2–8 pixels is set as a constraint, combined with the rules for selecting fitting starting points and hypothetical lowest points. As shown in Figure 2, lake profiles may exhibit multiple curve forms, making it difficult for a single curve-fitting function to represent complex and variable bathymetry. To address this issue, the model constructs a function library comprising multiple forms consistent with terrain variation characteristics, including linear functions, quadratic functions, exponential functions, trigonometric functions, and their variations. This function library aims to encompass the primary geometric forms that underwater topography may exhibit. Its core design philosophy is to map different mathematical forms to typical geomorphic features. Specifically, the linear function is suitable for areas with uniform slope, gentle topographic relief, and smooth terrain, such as gentle lakeshore slopes. The quadratic function can better fit profiles with concave or convex features and is commonly used to simulate bowl-shaped lake basins. The exponential function is applicable for depicting lake-bottom forms in which water depth changes rapidly near the shore or gradually stabilizes in the offshore area, especially for simulating steep fault scarps or silt-rich deepwater regions. The trigonometric function can be used to reflect the periodic fluctuations in bedform morphologies formed by glacial erosion or tectonic activity. During the calculation process, the model does not rigidly employ a single function but selects the most suitable function form or combination based on local topographic features extracted from the buffer zone. This selection mechanism ensures that the topographic extrapolation maintains the most reasonable continuity with adjacent terrain, enhancing the model's interpretability and robustness across different environments.

On the basis of the assumption that the longitudinal profiles of the lake exhibit continuity and by applying the extremum principle, it is inferred that at the hypothetical lowest point of the lake, the derivative equals zero, indicating that the slope is zero. This setting enables the model to adapt to different types of terrain variations while preserving bathymetric features as much as possible. Adopting the current calculation profile as an example, the model applies the above rules for fitting, selects the optimal profile function type, determines the function parameters by solving the derivative of the loss function, and ultimately chooses the function with the coefficient of determination closest to 1 as the best fitting function. During iteration, the model adaptively selects both the function form and its parameters.

Specific fitting process:

i) Minimization of the loss function. For each candidate function form $f(x,\theta)$, the objective of the model is to minimize the loss function.

$$S(\theta) = \sum_{i=1}^{n} (y_i - f(x_i,\theta))^2 \quad (4)$$

where (x_i, y_i) represents the DEM elevation, $f(x,\theta)$ denotes the fitting function, and θ refers to the parameters to be fitted.

ii) The loss function is differentiated to obtain the optimal parameters, and the coefficient of determination R^2 is calculated to evaluate the fitting performance.

$$R^2 = 1 - \frac{\sum_{i=1}^{n} (y_i - f(x_i,\theta))^2}{\sum_{i=1}^{n} (y_i - \bar{y})^2} \quad (5)$$

where $\bar{y}$ is the mean value of the DEM data, m. Based on the fitting results, the function with the coefficient of determination R^2 closest to 1 is selected as the optimal fitting function.

The hypothetical lowest point during elevation calculation is dynamically variable. In Figure 8, dashed lines A and B represent two consecutive elevation iterations, while the solid dots denote their corresponding hypothetical lowest points. For the current profile, the horizontal distances on both sides differ under the same descent gradient, resulting in a shift in the position of the lowest point. Therefore, to accurately describe bathymetric variation and ensure the rationality of the model simulation, the model recalculates the position of the lowest point in each iteration. Specifically, during every iteration,

the model fits a curve that better reflects the actual terrain. This dynamic adjustment not only improves accuracy but also enhances the adaptability of the model to different geomorphic characteristics.

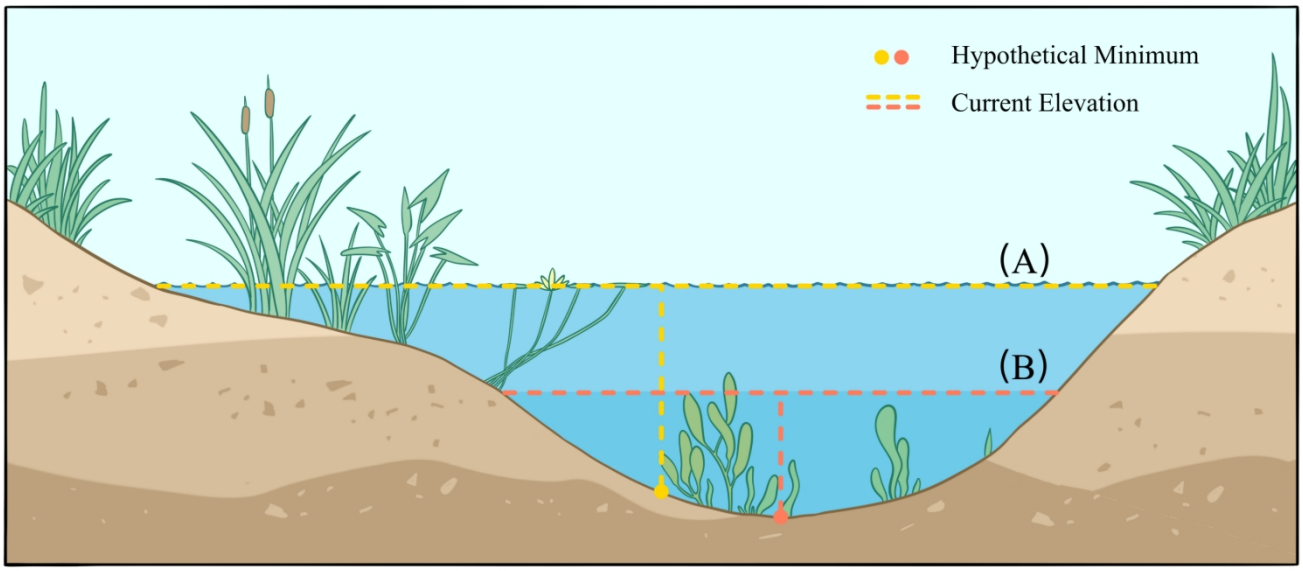

Figure 8. Schematic diagram of the lowest point iteration.

The slope of the current pixel is calculated using the fitted function, and its elevation is then determined according to Equation (6). For pixels with multiple adjacent directions, the results obtained from different directions are averaged, and the final value is recorded in the computed area. Moreover, the slope module is updated accordingly.

$$Z(i) = h1_i - k1_i \times \text{cellsize} \quad (6)$$

where $Z(i)$ represents the elevation of the current calculation pixel, m; *cellsize* is the raster resolution, m, which in this study is 90 m; and $h1_i$ is the elevation of the adjacent pixel along the calculation direction, m (during the first iteration of the model, $h1_i$ corresponds to the elevation of the neighbouring land pixel, m); and $k1_i$ is the slope of the current calculation pixel derived from the optimal fitting function.

(4) Sedimentation Calculation

According to the assumption proposed in Section 3.1.1, the lake sediment layer is among the primary factors causing discrepancies between the model simulation results and the measured results. To address this issue, a sedimentation coefficient is introduced to calculate the thickness of the lake sediment layer.

$$Sc = \frac{h_{data}}{h_{model}} \quad (7)$$

where *Sc* is the sedimentation coefficient, h_{data} is the measured or collected average depth of the lake, m, and h_{model} is the average depth from the natural surface to the water surface calculated by the model, m. For lakes lacking actual measurement data, a migration strategy for lake sedimentation coefficients across different categories can be adopted. The specific process is as follows: Select multidimensional feature indicators closely related to the sedimentation process, including geological basement type, watershed topographic attributes, land cover conditions, and lake morphological parameters. Then use hierarchical clustering to classify lake samples objectively. Apply the sedimentation coefficients calculated from lakes with actual measurement data within the same category to lakes lacking actual measurement data within the same group, thereby achieving indirect estimation of the sedimentation thickness of lakes without actual measurement data. The parameters employed in the formula are shown in Figure 9.

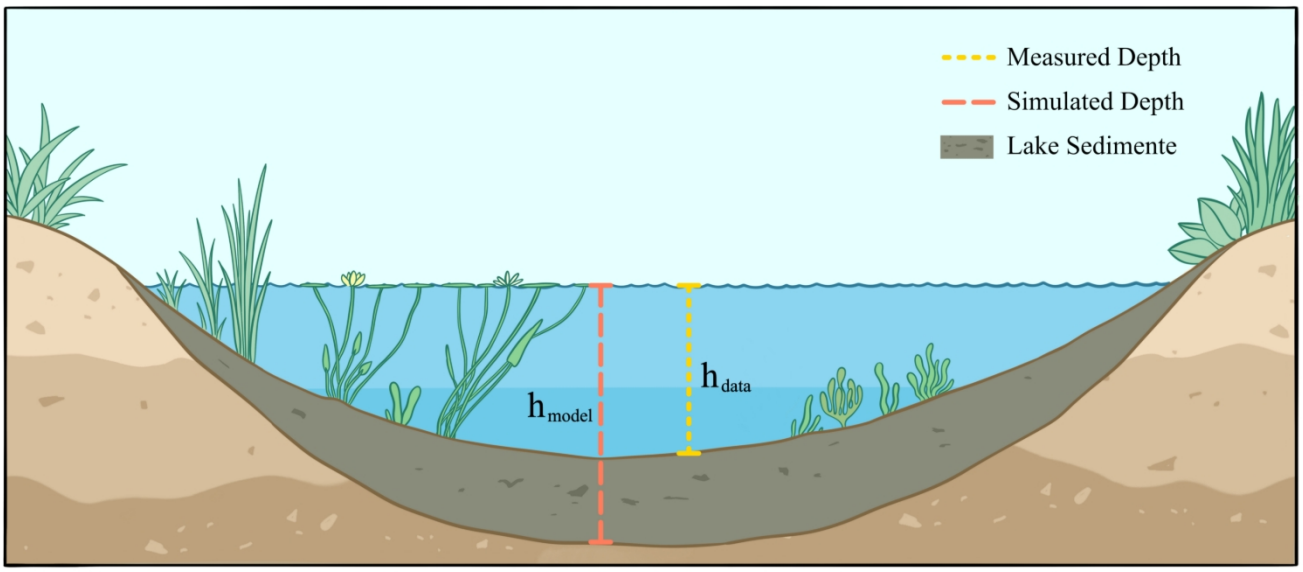

Figure 9. Lake sedimentary diagram.

3.2 Accuracy Evaluation

Bathymetry calculation accuracy: For lakes with measured data, the pixel-by-pixel comparison method is applied. The measured data are resampled to match the resolution of the model outputs. Water storage estimation accuracy: Cross-validation of the model results with the validation dataset The model accuracy is then quantitatively evaluated using indicators such as the coefficient of determination (R^2), relative error (RE), mean absolute error (MAE), and root mean square error (RMSE). For lakes without measured data, model accuracy is indirectly evaluated by comparing the average depth and maximum depth.

4. Results and Discussion

4.1 Accuracy Evaluation of Lake Depth Simulation

Comparisons of the maximum and average depths simulated by the model and measured data for each validation lake are provided in Table 2. In terms of average depth simulation accuracy, the model shows good stability for most lakes. Among the lakes, Salt Lake, Mapam Yumco, and Ra'ang Co exhibit relative errors in average depth that are all within 10%, with Salt Lake showing an error of only -7.5%, indicating the reliability of the model. This phenomenon is likely related to the relatively regular basin shapes of these lakes and the smooth surrounding terrain, which allows the extrapolation algorithm based on terrain feature similarity to perform effectively. Despite significant deviations in the estimated average depth in these lakes, the model still provides relatively accurate estimates. However, the model exhibited relatively large errors in smaller lakes (such as Xingxinghai and Kuhai Lake), especially in the calculation of average depth, with errors reaching 47% and -42.8%, respectively. It is worth noting, however, that the relative errors in maximum depth were much lower, at 9.1% and -17.7%, respectively. This discrepancy indicates that despite significant deviations in the estimation of average depth in these lakes, the model still provides relatively accurate results for the estimation of maximum depth. The reasons for this phenomenon may include the following: Firstly, the terrain's complexity in shallow-water areas is a primary factor. Small lakes usually have relatively complex shorelines and bottom morphologies, leading to more dramatic topographic changes in shallow water areas. These local details are challenging to capture with existing DEM data, leading to high errors in average depth estimation. Secondly, due to the small size of these lakes, the model may be affected by lower-resolution DEM data during processing, especially in shallow water areas. The limited resolution leads to a loss of detail, further increasing the error. Moreover, owing to the shallow depths of these lakes, even small absolute

errors between the simulated and measured values are significantly magnified in the relative error calculations.

With respect to the maximum depth simulation, the model is highly accurate for lakes such as Cuoe Lake and Salt Lake, with relative errors all within 20%. However, the errors significantly increase in larger, more complex lakes such as Yamdrok Lake and Dongge Co'nag. This difference likely arises due to the multibasin structure and complex underwater topography of large lakes. Specifically, the applicability of the traditional geological continuity assumption diminishes in complex tectonic lake areas, especially when lakes have multiple sediment centres or complex fault systems. The simple profile extrapolation method can hardly accurately replicate the real distribution of depth extremes in such areas. Notably, the model exhibits systematic performance differences across lakes of varying sizes: the simulation accuracy is generally greater for medium-sized lakes (200–500 km²), whereas larger (more than 500 km²) and smaller (less than 100 km²) lakes have greater errors. This scale effect reveals the inherent limitations of the current method; specifically, the terrain heterogeneity of small lakes and internal structural complexity of large lakes exceed the current processing capacity of the model. Additionally, the error distribution shows some regional clustering, which may be closely related to the geological structure and types of lake genesis in different regions. These findings provide possible directions for future model optimization.

Table 2. Sample lake accuracy comparison table.

Lake Name	Longitude (°)	Latitude (°)	Lake Area (km²)	Avg. Depth (Model, m)	Max. Depth (Model, m)	Avg. Depth (Measured, m)	Max. Depth (Measured, m)	RE (Avg. Depth, %)	RE (Max. Depth, %)
Anglaren Co	83.06	31.56	511.02	22.91	31.17	18.32	41.13	25.0	-23.9
Cuoe Lake	88.75	31.57	248.53	21.33	36.23	17.61	30.79	21.0	18.0
Ra’ang Co	81.22	30.70	248.31	20.76	42.38	23.23	49.03	-10.5	13.6
Mapam Yumco	81.45	30.68	410.56	42.34	59.73	46.34	81.82	-7.9	-26.9
Salt Lake	93.41	35.52	209.41	13.04	38.88	13.13	36.26	-7.5	8.0
Yamdrok Lake	90.66	28.93	542.19	27.68	31.27	23.61	59.18	17.2	-47.0
Dongge Co’nag	98.53	35.31	257.43	20.56	47.74	28.96	71.35	-29.0	-32.8
Xingxinghai	98.11	34.85	28.62	8.72	12.52	5.93	11.48	47.0	9.1
Kuhai Lake	99.17	35.33	48.67	4.31	15.30	7.54	18.63	-42.8	-17.7

For the four lakes with measured data, the pixel-by-pixel evaluation results are provided in Table 3. The model maintains reasonable accuracy across different types of lakes ($R^2 > 0.65$, RE < 20%), demonstrating the applicability of the underwater terrain reconstruction method based on terrain feature similarity in the Qinghai–Tibet Plateau region. Since the validation data are distributed along limited measurement lines, the evaluation results reflect the performance of the model along specific profile paths rather than a comprehensive evaluation of the entire topography of the lake basin.

In terms of overall accuracy, the model performs excellently for Ra'ang Co and Mapam Yumco, with R^2 values of 0.915 and 0.898, respectively, indicating that the model can accurately capture spatial variations in the lakebed topography. However, the R^2 value for Cuoe Lake is relatively low (0.677), suggesting that the lake may have localized complex terrain features, leading to relatively large

deviations in certain profile positions. Although Anglaren Co has the fewest validation points (194), its RMSE (2.835 m) and MAE (2.083 m) are the lowest among the four lakes, indicating high absolute accuracy in this lake. In contrast, the RMSE for Mapam Yumco reaches 5.950 m, which aligns with its greater water depth, suggesting increased prediction uncertainty in deeper water regions. However, given the significant depth variation in this lake, this error level remains within an acceptable range.

Notably, because the validation points are distributed along the measurement lines, the current evaluation results may not fully represent the overall topographic reconstruction accuracy of the lake. For example, Anglaren Co, which exhibits the fewest validation points (194), reveals the highest relative error (19.77%). This phenomenon may be closely related to the measurement line positions and local terrain complexity. Overall, while the model maintains reasonable accuracy in most lakes with limited validation data, a comprehensive assessment of the overall performance of the model will require future acquisition of more widely distributed measured data for supplementary validation.

Table 3. Error statistics of the model calculation results and measured data.

Lake Name	Number of Validation Points	RMSE (m)	RE (%)	MAE (m)	R^2
Ra'ang Co	1752	4.367	12.86	3.432	0.915
Cuoe Lake	988	4.506	15.73	3.459	0.677
Anglaren Co	194	2.835	19.77	2.083	0.798
Mapam Yumco	395	5.950	17.29	4.190	0.898

The spatial distribution of the errors between the model's simulation results and the observed data is shown in Figure 10. Overall, the model effectively captures the macroscale variations in lakebed topography, particularly in the zones of transition from shallow to deep water, which indicates that the model has a good ability to represent the extension features of the shore and surrounding terrain. However, in deep water areas, especially where abrupt changes occur in the underwater terrain, the model performance significantly decreases. This phenomenon is due primarily to three mechanisms. First, deep water areas usually lack sufficient data to constrain the model, forcing them to rely on extrapolation algorithms in the absence of effective observational information. Second, deep-water terrain is often controlled by geological processes distinct from those in shoreline areas, weakening the correlation between its morphological features and the surrounding terrain and reducing the reliability of extrapolation based on the geological continuity hypothesis. Importantly, the iterative calculation mechanism applied in the model leads to vertical error propagation; notably, the bias generated in earlier iterations is amplified in subsequent calculations, ultimately resulting in significant error accumulation in deep-water regions. The excellent performance of the model in shallow areas contrasts sharply with its limitations in deep water, highlighting the inherent limitations of the terrain feature similarity-based extrapolation method. While the method performs well in nearshore regions where the surrounding terrain strongly influences the lakebed, it faces applicability constraints in deep water areas dominated by internal lake basin processes.

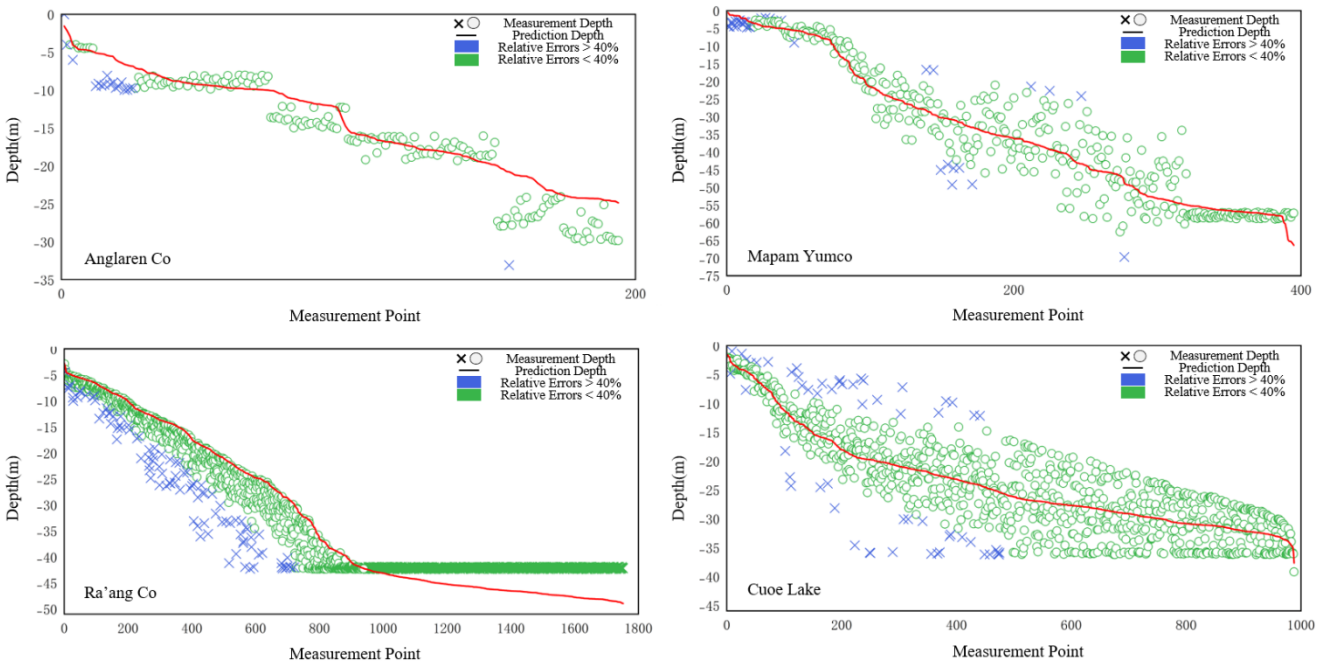

Figure 10. Error analysis of simulation results.

The results of error distribution analysis across different depth ranges are shown in Figure 11. In the shallow water zone (0–5 m), although the relative error is relatively high, the average absolute error remains less than 1.04 m, indicating that the model maintains good accuracy in shallow areas. The main reason for the larger relative errors is the small baseline depth in the shallow zone, which amplifies small absolute deviations in the relative error calculation. This phenomenon is particularly evident in the gentle slope areas at the edge of the lake.

In the transition zone (5-50 m), the model performs best, with the relative error remaining consistently below 20%. This depth range is where the terrestrial terrain transitions to underwater topography with the highest continuity, allowing the extrapolation algorithm of the model based on the geological continuity hypothesis to perform effectively. Additionally, this depth zone typically has moderate terrain variation, neither overly sensitive to small errors as in the shallow water zone nor experiencing the sudden terrain changes found in deep water zones. However, in deep-water regions (greater than 50 m), the model accuracy decreases systematically.

Moreover, the model tends to overestimate all depth ranges, potentially due to the inclination of the algorithm to maintain terrain continuity in the absence of strong constraints, thereby smoothing out local depressions in the actual terrain. To further evaluate the model's overestimation trend, we analyzed the mean squared error (MSE) across different depth intervals. The results showed that the model performed best in the shallow layer (0-5 m), with an MSE of only 0.57 m^2. In the middle layer (5-50 m), the MSE increased by an order of magnitude, with most interval errors between 1-5 m and an overall MSE of 5.15 m^2. The depth segments with larger errors in this layer are the 30-35 m and 45-50 m of Ra'ang Co. The deep layer (>50 m) only contains four depth layers of Mapam Yumco, with an MSE of 17 m^2. The error in the 65-70 m depth layer is particularly prominent, which is the main reason for the high MSE in this interval. This systematic bias reveals that the current model needs further optimization in terms of balancing terrain complexity and algorithm stability, especially in terms of handling complex geomorphologies in deep water areas, which requires the introduction of additional geological constraints.

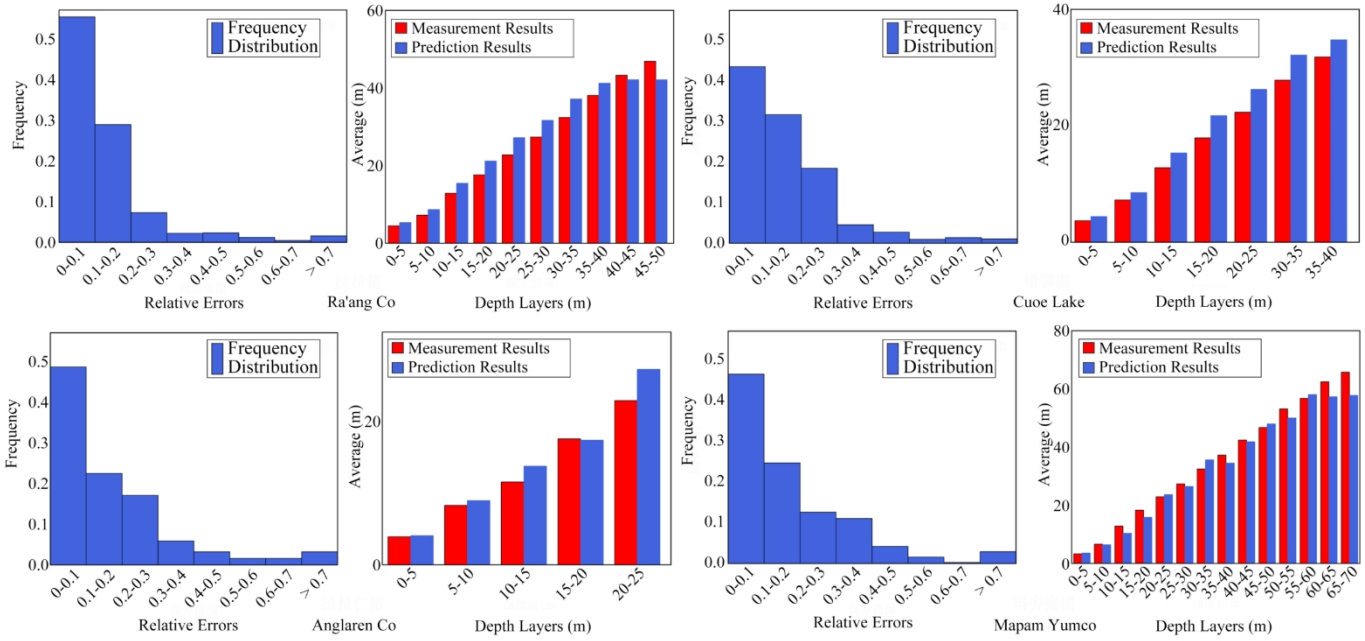

Figure 11. Histograms of the relative error absolute value frequency distribution of the lakes and comparative analyses of different depth layers.

4.2 Comparative Analysis of Lake Profiles

To further analyse potential issues in model predictions, five representative lake profiles were selected for comparative analysis (Figures 12 and 13).

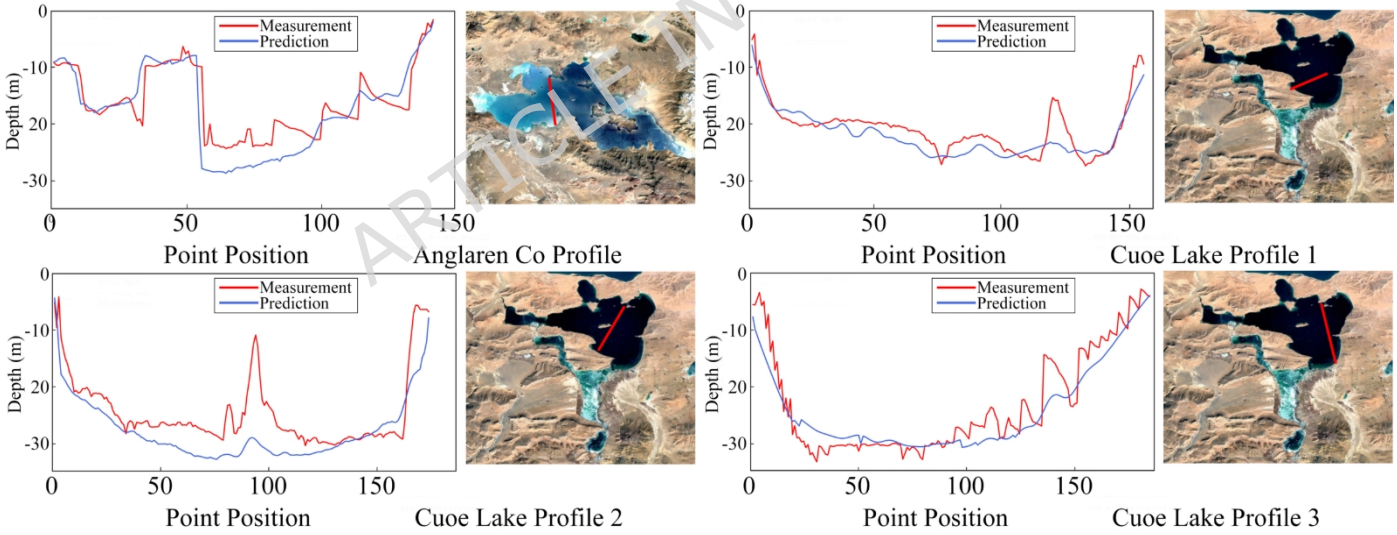

Figure 12. Comparison of lake profiles.

The model exhibits consistency in terms of the macro trends of the lakebed topography and smoothing of the micro features. Although the model can accurately reproduce the overall shape of the lake basin, its ability to depict fine topographical features such as local steep slopes and depressions remains inadequate. This limitation is partly due to the inherent precision constraints of the original DEM data and partly due to the design considerations of the model, in which some loss of fine detail is sacrificed to ensure the overall accuracy.

As shown in Figure 13, the first 20 validation points exhibit significant fluctuations, reflecting the challenges the model faces in managing vertical terrain changes. When the profile calculation

inadvertently incorporates the influence of valley terrain orthogonal to the current direction, short-term deviations in the simulation results occur. The model effectively controls the propagation of such errors through a dual mechanism: (1) by suppressing terrain features to maintain abnormal terrain changes within a certain range and (2) by relying on the adaptive fitting capabilities of the dynamic function library, which continuously corrects earlier deviations in subsequent iterations. This self-correction feature enables the model to progressively reduce local errors in long-profile calculations, ultimately achieving accurate reconstruction of the overall terrain trend. This design renders the model suitable for the preliminary reconstruction of underwater topography in large-scale, data-scarce regions, but it has limitations in scenarios where fine local topography must be captured.

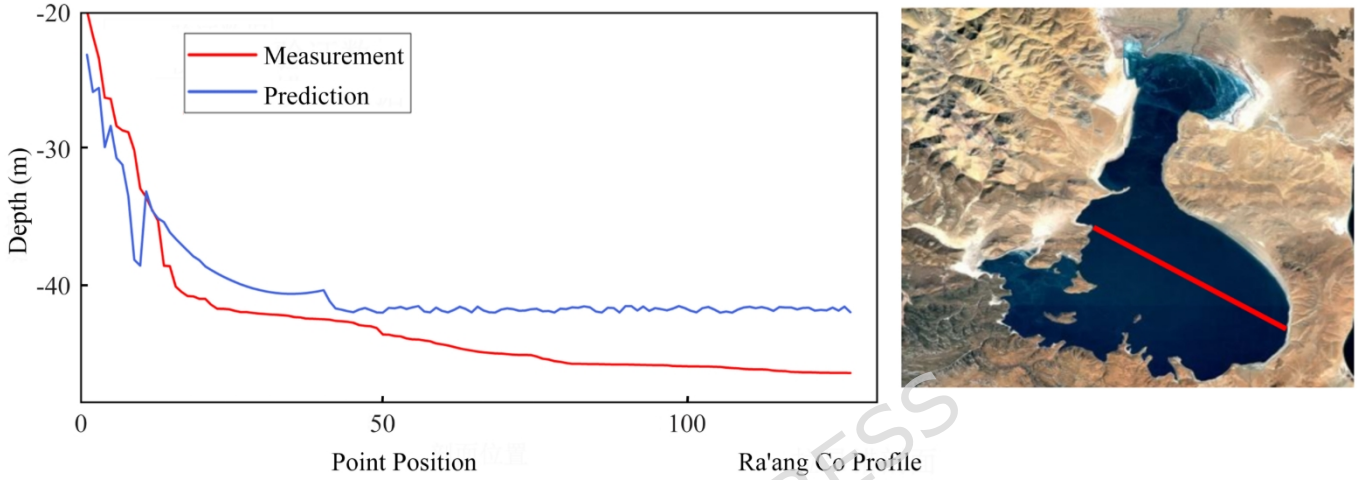

Figure 13. Comparison of lake profiles.

4.3 Lake Water Storage Accuracy Evaluation

The cross-validation results between the model-estimated water volume and the validation dataset (Table 4) reveal that the model performs excellently for large deep-water lakes such as Mapam Yumco, with a relative error of only -2.73%. In contrast, the simulation for Dongge Co'nag shows a significant deviation, with a relative error of -42.9%, indicating that the applicability of the model may have certain limitations for specific types of lakes. This performance disparity is likely related to the unique morphological characteristics of each lake. The relatively regular basin shape of Mapam Yumco enables the model to accurately simulate its topographical variations. However, Dongge Co'nag may have a relatively complex basin structure, such as multiple sedimentation centres and intricate shoreline features, which increase the uncertainty in terrain extrapolation and water storage estimation. Further analysis reveals that, except for Yamdrok Lake, the other lakes exhibit varying degrees of underestimation. This phenomenon may be due to the cumulative error effect in the iterative algorithm and the oversmoothing of the lake shoreline topography. Overall, the cross-validation results reveal that the model is highly accurate at estimating water storage for most lakes. However, specific lake characteristics need to be considered in practical applications. Furthermore, introducing additional prior knowledge can further improve estimation accuracy.

Table 4. Model water volume cross-validation.

Lake Name	Model Water Volume (billion m³)	Validation Water Volume (billion m³)	Absolute Error (billion m³)	Relative Error (%)
Anglaren Co	97.39	113.22	15.83	-13.99
Dongge Co'nag	40.43	70.81	30.38	-42.90
Mapam Yumco	168.16	172.87	4.71	-2.73
Yamdrok Lake	169.16	154.73	14.43	9.33

5. Issues and Prospects

5.1 Current Issues

The innovation of this study lies mainly in the integration of the multidirectional profile combination iterative algorithm with the dynamic function library, overcoming the limitations of traditional single-direction extrapolation methods. This approach enhances the adaptability of the model to complex terrains while maintaining robustness. However, this study reveals the limitations of the current method in deep-water areas and in specific lake basin shapes.

5.2 Prospects

To increase the accuracy and general applicability of the model in complex environments, future research can be focused on three directions. First, the introduction of high-resolution DEM data (such as 30 metres or 12.5 metres) can effectively increase the accuracy of the characterization of shoreline shapes and slope features, especially in small-scale lakes and complex terrain regions. Additionally, a complementary noise suppression mechanism should be developed, using adaptive filtering algorithms and slope variation threshold constraints to retain valid terrain signals while eliminating local fluctuations and measurement errors caused by high-resolution data. Second, a systematic lake morphology classification system should be established, with different parameter schemes that are based on different basin types. This characteristic is particularly important for developing specialized correction modules for deep-water areas and complex lake basin structures. Finally, A hybrid modeling framework of "physical mechanism guidance-data-driven correction" should be developed. The physical model provides the fundamental laws and boundary constraints of terrain evolution. At the same time, machine learning methods are used to optimize key parameters, identify local terrain anomalies, and correct preliminary inversion results. The two are dynamically adjusted through an iterative feedback mechanism: the output of the physical model serves as the input and constraint conditions for the machine learning module, and the corrected results from the machine learning module are fed back into the physical model to drive parameter adjustment and structural optimization. This "mechanism-data" dual-driven model can not only maintain the interpretability and physical consistency of the model, but also fully utilize the complex nonlinear information hidden in the data, thereby synergistically improving the rationality and spatial accuracy of underwater terrain inversion, providing reliable technical support for the sustainable management of plateau lake water resources.

Furthermore, embedding the generated lake basin topographic data into ecological models, such as "environmental controls on the conversion of nutrients to chlorophyll in lakes," can significantly enhance the predictive ability of spatiotemporal patterns of lake primary productivity. In the context of global warming, both the thermal structure of lakes and sediment-water interface exchange processes are deeply influenced by lake basin morphology. Therefore, high-resolution underwater topographic data will become a crucial input for accurately simulating lake biogeochemical cycles and ecosystem responses to climate change. This integration not only reflects the innovative value of geographic information technology in ecological modeling but also provides more reliable decision support for water resource management and ecological protection of plateau lakes.

6. Conclusions

In this study, a lake bottom topography reconstruction and water volume estimation method that is based on surrounding lake terrain parameters is proposed. By innovatively introducing a dynamic function library and a multidirectional neighbourhood iterative algorithm, the adaptability of the model to complex terrain and its calculation accuracy are significantly improved. Systematic validation considering nine representative lakes of the Qinghai–Tibet Plateau reveals the following:

Lake Bottom Topography Reconstruction:

The method demonstrates suitable accuracy and stability in reconstructing the underwater topography of the lake. For the four lakes with measured data, the relative error between the simulated

and measured results remains within 20%. Notably, in the 5–50 m transition zone, the model exhibits excellent stability. The validation results confirm the effectiveness and applicability of the method for plateau lakes.

Water Volume Estimation:

The cross-validation results reveal variability in model performance. For large deep-water lakes such as Mapam Yumco, the model results are highly consistent with the validation data, with an RE of only -2.73%. However, the accuracy of water volume estimation for lakes with complex basin shapes, such as Dongge Co'nag, is relatively low, reflecting the limitations of the model in handling complex basin structures. However, in most lake instances, the model systematically underestimates the water storage capacity. This conservative bias primarily stems from the tendency towards "smoothing" in multiple aspects of the algorithm design. Firstly, due to error propagation in the iterative computation process, any deviation in the preceding steps accumulates during the reconstruction of deep-water areas, leading to conservative terrain-estimation results. Secondly, in terms of function library selection and surface-fitting criteria, the preference for smooth, continuous curves in their mathematical form suppresses the depiction of microtopographic features, such as local steep changes or depressions, during the fitting process, thereby excessively smoothing out terrain details that contribute to water storage volume. Furthermore, the currently adopted slope homogenization method may also introduce smoothing biases. This method weakens the anisotropy of terrain slopes, especially by underestimating the true slopes of underwater terrain near steep shorelines, which, in turn, affects the subsequent calculation of overall water storage volume. The interlocking effects of these factors form a "smoothing chain" that runs through the algorithm: the already-smoothed initial input becomes even smoother after surface function fitting, and this smoothing effect is spatially propagated through iterative computation. Ultimately, the reconstructed lake basin terrain is flatter and more regular than the actual terrain, leading to a systematic underestimation of the model's estimation of water storage capacity. This process is the core mechanism driving the model's conservative bias. Therefore, future model improvements should focus on breaking this "smoothing chain". For example, consideration could be given to introducing terrain roughness constraints, developing anisotropic slope calculation methods, or incorporating mathematical models that can characterize local abrupt changes into the function library to reduce the algorithm's tendency to excessive smoothing of terrain.

Funding: This research was funded by the Geological Survey of China (GSC) project [Grant No. DD20220960].

Data Availability Statement: All the data used in this study are included within the article.

Conflicts of Interest: The authors declare that they have no conflicts of interest.

Author Contributions Statement：Xuteng Zhang was responsible for conceptualizing the study, developing the methodology, and drafting the manuscript. Changxian Qi and Dezhong Xu contributed to data collection, preprocessing, and analysis of remote sensing datasets. Yao Chen and Hongjun Li assisted in model construction, validation, and result visualization. Haiyue Peng supervised the overall research design, provided critical revisions, and guided the interpretation of results. All authors discussed the results, contributed to the final manuscript, and approved the submitted version.

References

1. AI B, WEN Z, WANG Z, et al. Convolutional neural network to retrieve water depth in marine shallow water area from remote sensing images[J]. IEEE Journal of Selected Topics in Applied Earth Observations and Remote Sensing, 2020, 13: 2888-2898.
2. ALPERS W, HENNINGS I. A theory of the imaging mechanism of underwater bottom topography by real and synthetic aperture radar [J]. Journal of Geophysical Research: Oceans, 1984, 89(C6): 10529-46.

3. BIAN X, SHAO Y, TIAN W, et al. Underwater topography detection in coastal areas using fully polarimetric SAR data [J]. Remote Sensing, 2017, 9(6): 560.
4. CALKOEN C, HESSELMANS G, WENSINK G, et al. The bathymetry assessment system: efficient depth mapping in shallow seas using radar images [J]. International Journal of Remote Sensing, 2001, 22(15): 2973-98.
5. COLLIN A, HENCH J L. Towards deeper measurements of tropical reefscape structure using the WorldView-2 spaceborne sensor [J]. Remote Sensing, 2012, 4(5): 1425-47.
6. DAI Y. F., WANG T., SHENG Y. W., et al. Intensified Lake Effects of the Tibetan Plateau under Global Warming [J]. Science Bulletin, 2024, 69(07): 968-977.
7. DAWA C. Impact of Global Climate Change on Water Resources of the Tibetan Plateau [J]. Tibet Studies, 2010, (04): 90-99.
8. FANG C, LU S, LI M, et al. Lake water storage estimation method based on similar characteristics of above-water and underwater topography [J]. Journal of Hydrology, 2023, 618: 129146.
9. Han, X., Zhang, G. (2024). Simulated lake volume dataset on the Tibetan Plateau (2022). National Tibetan Plateau / Third Pole Environment Data Center.
10. HEATHCOTE A J, DEL GIORGIO P A, PRAIRIE Y T, et al. Predicting bathymetric features of lakes from the topography of their surrounding landscape [J]. Canadian Journal of Fisheries and Aquatic Sciences, 2015, 72(5): 643-50.
    HOLLISTER J W, MILSTEAD W B, URRUTIA M A. Predicting maximum lake depth from surrounding topography [J]. PLoS One, 2011, 6(9): e25764.
11. KG F. Simulation study on the effect of wind on SAR imaging of shallow water bathymetry [J]. J Remote Sens, 2008, 12(5): 743-9.
12. LYZENGA D R. Remote sensing of bottom reflectance and water attenuation parameters in shallow water using aircraft and Landsat data [J]. International journal of remote sensing, 1981, 2(1): 71-82.
13. MOSES S A, JANAKI L, JOSEPH S, et al. Lake bathymetry from Indian Remote Sensing (P 6-LISS III) satellite imagery using artificial neural network model [J]. Lakes & Reservoirs: Research & Management, 2013, 18(2): 145-53.
14. MERRYMAN BONCORI J. Caveats Concerning the Use of SRTM DEM Version 4.1 (CGIAR-CSI) [J]. Remote Sensing, 2016, 8(10).
15. MESSAGER M L, LEHNER B, GRILL G, et al. Estimating the volume and age of water stored in global lakes using a geo-statistical approach [J]. Nature communications, 2016, 7(1): 13603.
16. O'CONNOR J E, HARDISON J H, COSTA J E. Debris flows from failures of Neoglacial-Age moraine dams in the Three Sisters and Mount Jefferson wilderness areas, Oregon[M]. US Geological Survey, 2001.
17. PENG H. Construction and Variation Analysis of Lake Water Level Series on the Qinghai–Tibet Plateau [D]. Xining, Qinghai University, 2022.
18. PI X, LUO Q, FENG L, et al. Mapping global lake dynamics reveals the emerging roles of small lakes [J]. Nature communications, 2022, 13(1): 5777.
19. QIN B, ZHOU J, ELSER J J, et al. Water depth underpins the relative roles and fates of nitrogen and phosphorus in lakes [J]. Environmental Science & Technology, 2020, 54(6): 3191-8.
20. SHUCHMAN R, LYZENGA D, MEADOWS G. Synthetic aperture radar imaging of ocean-bottom topography via tidal-current interactions: theory and observations [J]. International Journal of Remote Sensing, 1985, 6(7): 1179-200.
21. SONG C, HUANG B, KE L. Modeling and analysis of lake water storage changes on the Tibetan Plateau using multi-mission satellite data [J]. Remote Sensing of Environment, 2013, 135: 25-35.
22. VERPOORTER C, KUTSER T, SEEKELL D A, et al. A global inventory of lakes based on high-resolution satellite imagery [J]. Geophysical Research Letters, 2014, 41(18): 6396-402.
23. Wang, J. (2018). Bathymetric Data of Ngangla Ringco Lake (2017). National Tibetan Plateau / Third Pole Environment Data Center. https://doi.org/10.11888/Hydro.tpdc.270057. https://cstr.cn/18406.11.Hydro.tpdc.270057.
24. Wang, J. (2018). Bathymetric data of Co Ngoin Lake (2017). National Tibetan Plateau / Third Pole Environment Data Center. https://doi.org/10.11888/Hydro.tpdc.270060. https://cstr.cn/18406.11.Hydro.tpdc.270060.

25. Wang, J. (2018). Bathymetric data of Mapam Yumco Lake (2017). National Tibetan Plateau / Third Pole Environment Data Center. https://doi.org/10.11888/Hydro.tpdc.270079. https://cstr.cn/18406.11.Hydro.tpdc.270079.
26. Wang, J. (2018). Bathymetric data of Laangcuo Lake (2017). National Tibetan Plateau / Third Pole Environment Data Center. https://doi.org/10.11888/Hydro.tpdc.270018. https://cstr.cn/18406.11.Hydro.tpdc.270018.
27. WANG W. Z., HUANG D., LIU J. F., et al. Lake Water Level–Volume Changes and Attribution of Tangra Yumco during 1988–2018 Based on Landsat and Sentinel-3A Satellite Data [J]. Journal of Lake Sciences, 2020, 32(05): 1552-1563.
28. WOOLWAY R I, KRAEMER B M, LENTERS J D, et al. Global lake responses to climate change [J]. Nature Reviews Earth & Environment, 2020, 1(8): 388-403.
29. XU Y, LI J, WANG J, et al. Assessing water storage changes of Lake Poyang from multi-mission satellite data and hydrological models[J]. Journal of Hydrology, 2020, 590: 125229.
30. YANG L. Y. Glacier and Glacial Lake Monitoring and Outburst Flood Disaster Simulation Using Radar Remote Sensing [D]. Xi'an: Chang'an University, 2024.
31. YANG Z, DUAN S-B, DAI X, et al. Mapping of lakes in the Qinghai-Tibet Plateau from 2016 to 2021: trend and potential regularity [J]. International Journal of Digital Earth, 2022, 15(1): 1692-714.
32. YAO F, WANG J, YANG K, et al. Lake storage variation on the endorheic Tibetan Plateau and its attribution to climate change since the new millennium [J]. Environmental Research Letters, 2018, 13(6): 064011.
33. YAO T, BOLCH T, CHEN D, et al. The imbalance of the Asian water tower[J]. Nat Rev Earth Environ, 2022, 3: 618–632.
34. ZHANG G, YAO T, XIE H, et al. Estimating surface temperature changes of lakes in the Tibetan Plateau using MODIS LST data [J]. Journal of Geophysical Research: Atmospheres, 2014a, 119(14): 8552-8567.
35. ZHANG G, YAO T, XIE H, et al. Lakes' state and abundance across the Tibetan Plateau [J]. Chinese Science Bulletin, 2014b, 59(24): 3010-3021.
36. ZHANG G, YAO T, XIE H, et al. An inventory of glacial lakes in the Third Pole region and their changes in response to global warming [J]. Global and Planetary Change, 2015, 131: 148-157.
37. ZHANG X, MA Y, ZHANG J. Shallow water bathymetry based on inherent optical properties using high spatial resolution multispectral imagery [J]. Remote Sensing, 2020, 12(18): 3027.
38. ZHANG Y. Z., MA X. Y., LI Q., et al. Impact of Global Warming on the Productivity of Different Recharge-Type Lakes on the Tibetan Plateau [J]. Scientia Geographica Sinica, 2024, 44(02): 351-358.
39. ZHOU J, WANG L, ZHANG Y, et al. Exploring the water storage changes in the largest lake (S elin C o) over the T ibetan P lateau during 2003–2012 from a basin-wide hydrological modeling[J]. Water Resources Research, 2015, 51(10): 8060-8086.
40. ZHU L. P., QIAO B. J., YANG R. M., et al. New Understanding of Water Quantity and Water Quality Changes in Lakes on the Tibetan Plateau [J]. Nature Journal, 2017, 39(3): 166-172.
41. ZHU S, LIU B, WAN W, et al. A new digital lake bathymetry model using the step-wise water recession method to generate 3D lake bathymetric maps based on DEMs [J]. Water, 2019, 11(6): 1151.